

Type Ia supernovae in the star formation deserts of spiral host galaxies

A. A. Hakobyan,^{1*} A. G. Karapetyan,^{1*} L. V. Barkhudaryan,¹ M. H. Gevorgyan¹ and V. Adibekyan^{2,3}

¹Center for Cosmology and Astrophysics, Alikhanian National Science Laboratory, 2 Alikhanian Brothers Str., 0036 Yerevan, Armenia

²Instituto de Astrofísica e Ciências do Espaço, Universidade do Porto, CAUP, Rua das Estrelas, 4150-762 Porto, Portugal

³Departamento de Física e Astronomia, Faculdade de Ciências, Universidade do Porto, Rua do Campo Alegre, 4169-007 Porto, Portugal

Accepted 2021 May 5. Received 2021 April 10; in original form 2021 January 7

ABSTRACT

Using a sample of nearby spiral galaxies hosting 185 supernovae (SNe) Ia, we perform a comparative analysis of the locations and light curve decline rates (Δm_{15}) of normal and peculiar SNe Ia in the star formation deserts (SFDs) and beyond. To accomplish this, we present a simple visual classification approach based on the UV/H α images of the discs of host galaxies. We demonstrate that, from the perspective of the dynamical timescale of the SFD, where the star formation (SF) is suppressed by the bar evolution, the Δm_{15} of SN Ia and progenitor age can be related. The SFD phenomenon gives an excellent possibility to separate a subpopulation of SN Ia progenitors with the ages older than a few Gyr. We show, for the first time, that the SFDs contain mostly faster declining SNe Ia ($\Delta m_{15} > 1.25$). For the galaxies without SFDs, the region within the bar radius, and outer disc contain mostly slower declining SNe Ia. To better constrain the delay times of SNe Ia, we encourage new studies (e.g. integral field observations) using the SFD phenomenon on larger and more robust datasets of SNe Ia and their host galaxies.

Key words: supernovae: individual: Type Ia – galaxies: bar – galaxies: disc – galaxies: star formation – galaxies: stellar content.

1 INTRODUCTION

It is believed that the progenitor of Type Ia supernova (SN Ia) is a carbon–oxygen white dwarf (WD) in close binaries, whose properties and explosion channels are still under debate (e.g. Livio & Mazzali 2018). SNe Ia show an important relation between the luminosity at *B*-band maximum and their light curve (LC) decline rate Δm_{15} : faster declining SNe are fainter (Phillips 1993). The Δm_{15} is the difference in magnitudes between the maximum and 15 d after, and is considered as a practically extinction-independent parameter (e.g. Hakobyan et al. 2020, hereafter H20). Much work has been done to determine the nature of SN Ia progenitors by studying the relations between the properties of SNe Ia and characteristics of galaxies in which they are discovered (e.g. Gallagher et al. 2005; Gupta et al. 2011; Rigault et al. 2013; Uddin et al. 2017; Kang et al. 2020). In particular, the SN Ia LC decline rate can be linked to the global age of host galaxy (e.g. Shen et al. 2017), which is usually considered as a rough proxy for the SN Ia delay time (i.e. time interval between the progenitor formation and its subsequent explosion). Recently, in H20, we showed that the correlation between the Δm_{15} of normal SNe Ia and hosts' global age appears to be due to the superposition of at least two distinct populations of faster and slower declining SNe Ia from older and younger stellar populations, respectively. For the most common peculiar SNe Ia, we showed that 91bg-like (subluminous and fast declining) events probably come only from the old population, while 91T-like (overluminous and slow declining) SNe originate only from the young population of galaxies. Such results have been obtained also from more accurate age estimations of SNe Ia host populations, using the local properties for SN sites (e.g. Rigault et al. 2013; Panther et al. 2019;

Rose et al. 2019). Eventually, the SN LC properties, delay time distribution (DTD), and relations with other host characteristics allow to constrain the SN Ia progenitor scenarios (see discussion in H20).

In this *Letter*, for the first time, we link the Δm_{15} of SN Ia with the progenitor age from the perspective of star formation desert (SFD) phenomenon. In short, the SFD, observed in some spiral galaxies (e.g. James & Percival 2015, 2018), is a region swept up by a strong bar with almost no recent star formation (SF) on both sides of the bar. There are increasing evidences in observations and simulations that SFD consists of old stars, and the quenching of SF in this region was due to the bar formation (e.g. Donohoe-Keyes et al. 2019; George et al. 2020), which dynamically removed gas from SFD over a timescale of ~ 2 Gyr (e.g. Donohoe-Keyes et al. 2019). The bar can show SF through its length, or SF can be found only at the bar ends, or the entire bar might not show SF (e.g. Díaz-García et al. 2020). Some bars might even dissolve during the evolution (e.g. Shen & Sellwood 2004), leaving the central SFD in galactic disc. On the other hand, it can be considered that the SFD is practically not contaminated by the radial migration of young stars from the outer disc (e.g. Minchev et al. 2018). Therefore, from the dynamical age-constrain of SFD ($\gtrsim 2$ Gyr), we consider that the DTD of its SNe Ia is truncated on the younger side, starting from a few Gyr, in comparison with those outside the SFD, where mostly young/prompt SNe Ia occur (delay time of ~ 500 Myr, Raskin et al. 2009). Given this, and if the progenitor's age is the main driver of the decline rate, the SNe Ia discovered in the SFDs should have faster declining LCs. In this study, we simply demonstrate the validity of this assumption according to the picture briefly described above, which provides an excellent new opportunity to constrain the nature of SN Ia progenitors.

* E-mail: artur.hakobyan@yerphi.am (AAH); a.karapetyan@yerphi.am (AGK)

2 SAMPLE SELECTION AND REDUCTION

We selected the sample for our study from a well-defined sample of H20, which includes data on the spectroscopic subclasses of nearby (≤ 150 Mpc) SNe Ia (normal, 91T-, 91bg-like, etc.) and their B -band LC decline rates (Δm_{15}), as well as homogeneous data on the host galaxies (distance, corrected $ugriz$ magnitudes, morphological type, bar detection, etc). The SFDs are observed in some barred Sa–Scd galaxies (e.g. James & Percival 2015, 2018), therefore we restricted the morphologies of SNe hosts to the mentioned types, with barred and unbarred counterparts. We also ignored hosts with strong morphological disturbances, which may add undesirable projection effects and complicate the assignment of an SN Ia to the SFD.

As seen in Wang et al. (1997); Anderson et al. (2015); Hakobyan et al. (2016), the vast majority of SNe Ia in spiral galaxies belong to the disc, rather than the bulge (spherical) component. Here, we checked this observational fact for the most common SN Ia subclasses separately. If SNe Ia belong mostly to the disc component, where SFD can be located, one would expect that the distributions of projected and R_{25} -normalized galactocentric distances¹ of SNe Ia along major ($|U|/R_{25}$) and minor ($|V|/R_{25}$) axes would be different, being distributed closer to the major axis (i.e. smaller $\langle |V|/R_{25} \rangle$) in comparison with $\langle |U|/R_{25} \rangle$, see Hakobyan et al. 2016, for more details). Table 1 shows the results of the two-sample Kolmogorov–Smirnov (KS) and Anderson–Darling (AD) tests on the comparison of the major versus minor axes distributions of 238 SNe Ia (based on a subsample from H20). The P -values of the tests suggest that the SNe Ia distribution along the major axis is inconsistent with that along the minor axis in Sa–Scd host galaxies with different inclinations, showing that the SN Ia subclasses in these hosts originate mostly from the disc population.

It should be noted that, because of the absorption and projection effects in the discs, the SFDs are observed in some spiral galaxies only with low/moderate inclinations (e.g. James & Percival 2015, 2018). Therefore, we also limited our host galaxy sample to inclinations $i < 70^\circ$. In total, there are 185 normal, 91T- and 91bg-like SNe Ia meeting the above criteria, of which 79 and 106 events have barred and unbarred hosts, respectively. These SNe Ia are discovered in 180 host galaxies, five of which host two events in each.

For these host galaxies, we used archival Galaxy Evolution Explorer (GALEX) far- and near-UV (Martin et al. 2005), *Swift* UV (Romig et al. 2005), and available $H\alpha$ images (e.g. Sánchez-Menguiano et al. 2018) to visually classify the morphology of their ionized discs into four SF classes: *i*) SF is distributed along the entire length of unbarred disc, from the center to the edge (97 SNe Ia hosts); *ii*) like in the first case, but for barred disc, SF along the bar, without SFD (36 objects); *iii*) SF along the bar, or SF might occur only at the bar ends, with SFD (43 objects); *iv*) SF is distributed along the unbarred disc, except the central SFD (9 objects). In all the cases, the circumnuclear SF is also possible. The r -band and UV images representing the classes² of galaxies can be found in Fig. 1. Note that the cosmic surface brightness dimming is insignificant for our galaxy sample, since hosts’ $z \lesssim 0.036$ ($\langle z \rangle = 0.017 \pm 0.009$).

Based on the optical g -band images, we measured bar radii of host galaxies using ellipse fitting to the bar isophotes with maximum ellipticity (see Díaz-García et al. 2016 and references therein, for more details on the bar radius measurement method). Then we deprojected

¹ Normalized to the g -band 25th magnitude isophotal semimajor axis of host galaxy ($R_{25} = D_{25}/2$).

² With some differences, a similar visual classification is also proposed by Díaz-García et al. (2020).

Table 1. Comparison of the projected and normalized distributions of the SN Ia subclasses along major (U) and minor (V) axes of Sa–Scd hosts.

| SN | N_{SN} | Subsample 1 $\langle U /R_{25} \rangle$ | vs | Subsample 2 $\langle V /R_{25} \rangle$ | $P_{\text{KS}}^{\text{MC}}$ | $P_{\text{AD}}^{\text{MC}}$ |
|--------|-----------------|---|----|---|-----------------------------|-----------------------------|
| Normal | 196 | 0.32±0.02 | vs | 0.20±0.02 | <0.001 | <0.001 |
| 91T | 27 | 0.38±0.06 | vs | 0.20±0.03 | 0.018 | 0.021 |
| 91bg | 15 | 0.34±0.06 | vs | 0.18±0.06 | 0.020 | 0.037 |

Notes: The $P_{\text{KS}}^{\text{MC}}$ ($P_{\text{AD}}^{\text{MC}}$) is the two-sample KS (AD) test probability that the distributions are drawn from the same parent sample, using a Monte Carlo (MC) simulation with 10^5 iterations as explained in H20. The respective mean values and standard errors are listed. The statistically significant differences ($P \leq 0.05$) between the distributions are highlighted in bold.

Table 2. Numbers of the SN Ia subclasses according to their locations in the SFD of Sa–Scd hosts or beyond.

| SNe Ia in \tilde{r}_{SN} | class i disc >0 | outer disc $\geq \tilde{r}_{\text{dem}}$ | bar/SF < \tilde{r}_{dem} | SFD < \tilde{r}_{dem} | All |
|--------------------------------------|----------------------|---|--------------------------------------|-----------------------------------|-----|
| Normal | 75 | 52 | 12 | 12 | 151 |
| 91T | 19 | 4 | 1 | 0 | 24 |
| 91bg | 3 | 5 | 0 | 2 | 10 |
| All | 97 | 61 | 13 | 14 | 185 |

each bar radius for host inclination and normalized it to the disc radius, i.e. $\tilde{r}_{\text{bar}} = R_{\text{bar}}/R_{25}$. For unbarred hosts with the central SFD (class *iv* in Fig. 1), we used the UV images to roughly estimate the radii of SFDs ($\tilde{r}_{\text{SFD}} = R_{\text{SFD}}/R_{25}$), where almost no UV fluxes are detected. Note that for our sample $\langle \tilde{r}_{\text{SFD}} \rangle \approx \langle \tilde{r}_{\text{bar}} \rangle = 0.30$. For further simplicity, we define a demarcation radius as:

$$\tilde{r}_{\text{dem}} = \begin{cases} \tilde{r}_{\text{bar}}, & \text{for } ii \text{ and } iii \text{ disc classes,} \\ \tilde{r}_{\text{SFD}}, & \text{for } iv \text{ class.} \end{cases}$$

For SNe Ia, we deprojected and normalized their galactocentric distances as well, i.e. $\tilde{r}_{\text{SN}} = R_{\text{SN}}/R_{25}$ (see Hakobyan et al. 2016).

Based on the host disc classification and the definition of demarcation radius, we grouped SNe according to their locations as follows: 97 SNe Ia are found in the disc of galaxies without a bar or SFD; 61 SNe are in the outer disc of hosts, which have either a bar or SFD; 13 SNe are found in bar or star-forming regions inside \tilde{r}_{dem} ; and 14 SNe Ia are in SFD. Table 2 displays the distribution of the SN Ia subclasses according to their locations in the SFD³ or beyond.

3 RESULTS AND DISCUSSION

With the aim of linking the Δm_{15} of SN Ia with the progenitor age, we study the SN decline rates that exploded in SFDs and other regions of hosts. In addition, we compare the SN galactocentric distances between the spectroscopic subclasses, and check the possible correlations between the Δm_{15} and galactocentric distances.

3.1 SNe Ia in the SFDs and beyond

To link the LC properties of SN Ia with the progenitor age from the perspective of the dynamical age-constrain of SFD, in Table 3,

³ Although detailed measurements of the underlying fluxes at SNe locations are beyond the scope of this Letter, nevertheless, for our confidence, we checked the vicinity of 14 SNe Ia in the SFDs simply using different apertures on the fits images, and found no detectable underlying UV/ $H\alpha$ fluxes.

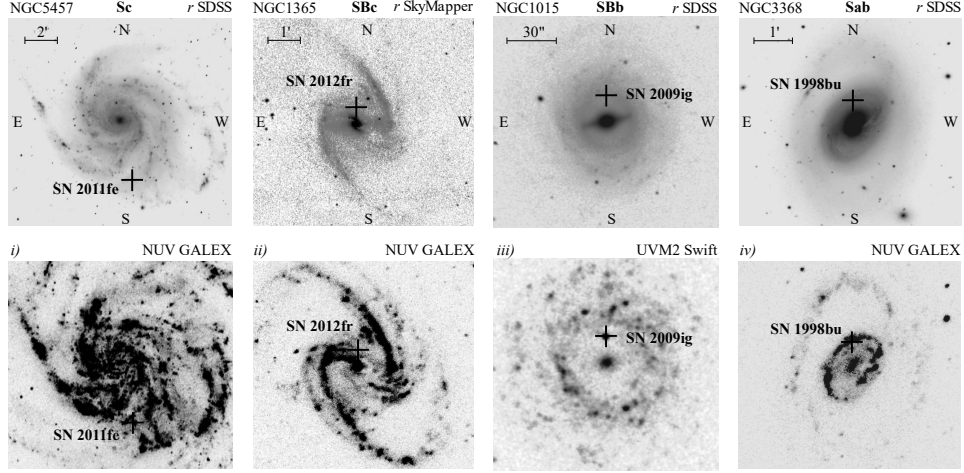


Figure 1. Optical (top) and UV images (bottom) representing examples of SN Ia hosts with different SF classes of their discs. Galaxies’ identifiers, morphologies, and discs’ classes are listed at the top. Classes *i* and *ii* do not have SFD, while classes *iii* and *iv* have SFD. SN Ia names/positions are also shown.

Table 3. Comparison of the B -band Δm_{15} distributions between normal SNe Ia in different locations (as described in Table 2).

| Subsample 1 | | | vs | Subsample 2 | | | P_{KS}^{MC} | P_{AD}^{MC} |
|---------------------------|----------|---------------------------------|----|---------------------------|----------|---------------------------------|---------------|---------------|
| SN in | N_{SN} | $\langle \Delta m_{15} \rangle$ | | SN in | N_{SN} | $\langle \Delta m_{15} \rangle$ | | |
| SFD | 12 | 1.32 ± 0.08 | vs | bar/SF | 12 | 1.07 ± 0.05 | 0.005 | 0.020 |
| SFD | 12 | 1.32 ± 0.08 | vs | outer disc | 52 | 1.13 ± 0.03 | 0.009 | 0.029 |
| bar/SF | 12 | 1.07 ± 0.05 | vs | outer disc | 52 | 1.13 ± 0.03 | 0.660 | 0.682 |
| SFD+bar/SF | 24 | 1.20 ± 0.05 | vs | outer disc | 52 | 1.13 ± 0.03 | 0.445 | 0.477 |
| inner class <i>i</i> disc | 17 | 1.19 ± 0.05 | vs | outer class <i>i</i> disc | 58 | 1.11 ± 0.02 | 0.517 | 0.253 |

Notes: Since, the $\langle \tilde{r}_{dem} \rangle = 0.30$ for class *ii-iv* discs, we define inner and outer class *i* discs when $\tilde{r}_{SN} < 0.30$ and ≥ 0.30 , respectively. The explanations for P -values are the same as in Table 1.

we compare the Δm_{15} distribution of normal SNe Ia in the SFD with that in the bar/SF (see also the upper panel of Fig. 2). The KS and AD tests show that these distributions are significantly different. Normal SNe Ia that are in the SFD, dominated by the old population ($\gtrsim 2$ Gyr; Donohoe-Keyes et al. 2019), have, on average, faster declining LCs compared to those located in the bar/SF, where UV/ $H\alpha$ fluxes are observed (i.e. age \lesssim a few 100 Myr; Kennicutt 1998).

Table 3 also shows that the Δm_{15} distribution of normal SNe Ia that are in the outer disc population is consistent with that in the bar/SF and inconsistent with that in the SFD (see also Fig. 2). Interestingly, any inconsistency vanishes when we combine the bar/SF and SFD subsamples and compare the LC decline rates with those in the outer disc population (Table 3). This suggests that the discs of Sa–Scd hosts are indeed outnumbered by normal SNe Ia with slower declining LCs (e.g. $\Delta m_{15} < 1.25$, outside the \tilde{r}_{dem} in Fig. 2) whose progenitor ages peak below 1 Gyr, corresponding to the young/prompt SNe Ia (e.g. Childress et al. 2014).

In addition, even for discs of class *i* (without demarcation radius), the KS and AD tests, in Table 3, show that the Δm_{15} distributions are consistent for normal SNe Ia in the inner and outer discs, excluding a radial dependency of Δm_{15} (see also Section 3.2). For class *i* discs, the $\langle \Delta m_{15} \rangle$ values are sufficiently consistent with the same values in the corresponding radial intervals for hosts having a demarcation radius (see Table 3). Thus, the SFD phenomenon gives an excellent possibility to separate a subpopulation of normal SNe Ia with old progenitors from a general population of host galactic disc, which contains both young and old progenitors. On average, the LCs

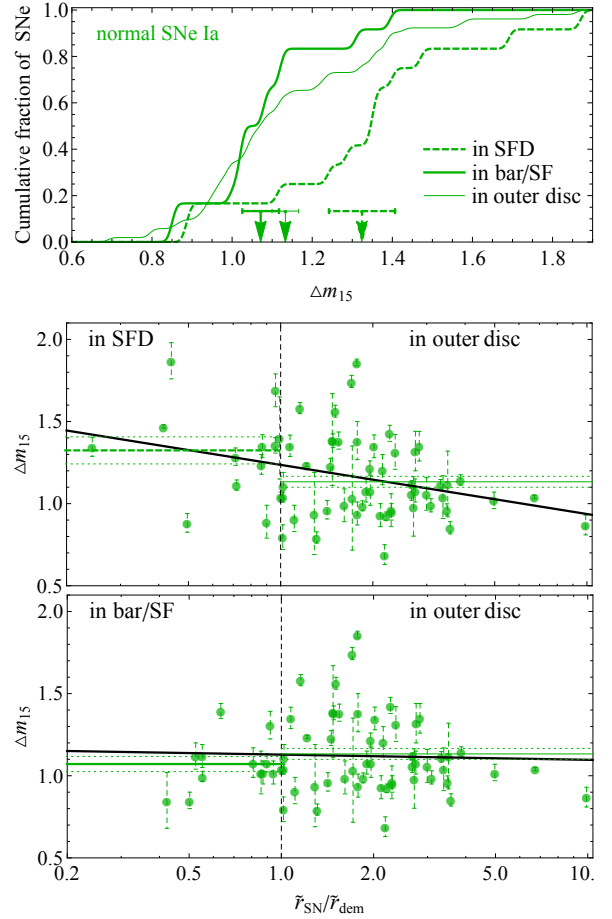


Figure 2. Upper panel: cumulative Δm_{15} distributions for normal SNe Ia inside (in SFD and bar/SF) and outside the demarcation radius (in outer disc). Bottom panel: variation of the Δm_{15} as a function of \tilde{r}_{dem} -normalized galactocentric distance, split between different SN locations. The best-fits are shown by thick (black) solid lines. The vertical dashed line indicates the location of radial demarcation (see the text for details). The mean values (with standard errors) of the distributions are shown by arrows (with error bars) in the upper panel, and by horizontal lines in the bottom panel.

of this SN Ia subpopulation decline faster, whose DTD is most likely truncated on the younger side, starting from a several Gyr ($\gtrsim 2$ Gyr).

These results are qualitatively agree with the theoretical predictions. In particular, for sub-Chandrasekhar mass ($M_{\text{Ch}} \approx 1.4M_{\odot}$) explosion models in double WD systems, the luminosity of SN Ia is directly related to the exploding WD's mass, which decreases with age (e.g. [Sim et al. 2010](#); [Blondin et al. 2017](#); [Shen et al. 2017, 2021](#)). This is because WD's mass is directly linked to the main-sequence (MS) mass of the progenitor star, which is in turn related to the MS lifetime. Therefore, older stellar populations would host less luminous SNe Ia, i.e. faster declining events (e.g. [Shen et al. 2017](#)). Note that, we prefer sub- M_{Ch} explosion models, because different mechanisms of the M_{Ch} explosions do not reproduce the observed distribution in the luminosity–decline rate relation for various SN Ia subclasses (e.g. [Livio & Mazzali 2018](#) and references therein).

Despite the small number statistics of peculiar 91T- and 91bg-like SNe, Table 2 shows that the old SFDs of Sa–Scd galaxies host along with faster declining normal SNe Ia also two 91bg-like (fast declining) events. While the bar/SF hosts along with slower declining normal events also one 91T-like (slow declining) SNe. Outer disc population hosts all the SN Ia subclasses (see Table 2). The latter is also correct for the entire class *i* disc. These results can be explained from the perspective of the SFD's properties in addition to the previously known relations between the SNe Ia and the global (or SN local) properties of their hosts.

In particular, the discovery of 91bg-like events (progenitor age is greater than several Gyr, e.g. [Crocker et al. 2017](#); [Panther et al. 2019](#); [Barkhudaryan et al. 2019](#); [H20](#)) and a population of faster declining normal SNe Ia in the SFDs can be explained within the scenario of SF suppression by bar, where the SFDs of galaxies show a sharp truncation in SF histories and contain mostly old stellar population of several Gyr ($\gtrsim 2$ Gyr; [Donohoe-Keyes et al. 2019](#)). On the other hand, the discovery of 91T-like SNe (progenitor age is less than a Gyr, e.g. [Han & Podsiadlowski 2004](#); [Ruiter et al. 2013](#); [Fisher & Jumper 2015](#)) and a population of slower declining normal events in the bar/SF (Tables 2-3), can be explained in the context of SF suppression scenario, where the recently formed bar, within the ~ 1.5 Gyr timescale, has not yet completely removed the gas and quenched ongoing SF inside the demarcation radius ([Donohoe-Keyes et al. 2019](#)). Recall that in the bar/SF regions, the UV fluxes are observed that trace the SF up to a few 100 Myr ([Kennicutt 1998](#)).

The outer disc of Sa–Scd galaxies (or entire class *i* disc), contains stellar populations of all ages (e.g. [González Delgado et al. 2015](#)). Therefore, the appearance of all the SN Ia subclasses in this region is not unexpected (Table 2). Note that the results in Table 3 remain statistically unchanged when we combine (following [Shen et al. 2017](#)) normal, 91T-, and 91bg-like SNe together.

To test different galaxy properties that could affect the results in Tables 2-3, we compare the distributions of morphologies, masses, colours, and ages (available in [H20](#)) of classes *ii-iv* hosts with and without SFD. The KS and AD tests show that the global parameters of hosts are not statistically different ($P > 0.1$), thus could not be the main drivers behind our results. On the other hand, the bar/SF regions have higher surface brightness and dust content in comparison with the SFDs, and therefore the discovery of intrinsically faint (faster declining) SNe in the bar/SF can be complicated, biasing the statistical results in Table 3. However, this does not affect the result that the SFD's SNe Ia are mostly faster declining (fainter) events.

Let us now briefly address the possible effects of the progenitor metallicity, which theoretically might cause a variation in the SN Ia LC properties. The mean radial metallicity profile of Sa–Scd galaxies declines from solar to ~ 0.3 dex below solar from the galactic

Table 4. Spearman's rank correlation test for the *B*-band Δm_{15} values of the SN Ia subclasses versus their galactocentric distances.

| SN | Galactocen. dist. | N_{SN} | r_s | P_s^{MC} |
|--------------------------------|--|-----------------|--------|-------------------|
| Normal | \tilde{r}_{SN} | 151 | −0.070 | 0.394 |
| 91T | \tilde{r}_{SN} | 24 | 0.087 | 0.686 |
| 91bg | \tilde{r}_{SN} | 10 | 0.503 | 0.138 |
| Normal (SFD+outer disc) | $\tilde{r}_{\text{SN}}/\tilde{r}_{\text{dem}}$ | 64 | −0.280 | 0.025 |
| Normal (bar/SF+outer disc) | $\tilde{r}_{\text{SN}}/\tilde{r}_{\text{dem}}$ | 64 | 0.019 | 0.879 |
| Normal (SFD+bar/SF+outer disc) | $\tilde{r}_{\text{SN}}/\tilde{r}_{\text{dem}}$ | 76 | −0.147 | 0.206 |

Notes: Coefficient r_s ($\in [-1; 1]$) is a measure of rank correlation. The variables are not independent when $P \leq 0.05$. The P_s^{MC} values are obtained using permutations with 10^5 MC iterations.

centre up to the disc end, respectively (e.g. [González Delgado et al. 2015](#)). On the other hand, the simulation by [Di Matteo et al. \(2013\)](#) shows that the metallicity on both sides of the bar, i.e. in SFD, is only ~ 0.15 dex below solar. For any progenitor model, such metallicity variations can account for less than 0.2 mag in SN Ia maximum brightness and about 0.1 mag in Δm_{15} (e.g. [Timmes, Brown & Truran 2003](#); [Kasen, Röpke & Woosley 2009](#)), which is not enough to be the main reason for the observed differences in Δm_{15} values in SFD and beyond (Fig. 2 and Table 3). Thus, our results support earlier suggestions that the progenitor age is most probably the decisive factor shaping the observed distribution of SN Ia decline rates (e.g. [Gallagher et al. 2005](#)). Nevertheless, we would like to stress that the discussed effect of metallicity is heavily based on a very limited number of models. Therefore, further modelling of the impact of metallicity on the LC properties of SNe Ia would help to place our findings in context.

3.2 The radial distribution of SNe Ia

In spiral discs, a radial gradient of physical properties of stellar population (e.g. age gradient; [González Delgado et al. 2015](#)) might be a useful tool and has been used in the past to probe the possible dependencies of SNe Ia decline rates on their galactocentric distance (e.g. [Gallagher et al. 2005](#); [Galbany et al. 2012](#); [Uddin et al. 2017](#)). However, in these studies, the authors were unable to find a significant correlation between the decline rate and \tilde{r}_{SN} , which is correct also for our sample (Table 4). Moreover, the radial distributions of peculiar (extreme decliners) and normal SNe Ia in Sa–Scd galaxies are consistent with one another ($P > 0.2$) (e.g. [Pavlyuk & Tsvetkov 2016](#)). Note that these results remain statistically insignificant ($P > 0.1$) when we perform the same tests after separating the hosts into barred/unbarred, and early/late-types. The Δm_{15} is not correlated with \tilde{r}_{SN} ($P > 0.4$) also for the class *i* disc only, where no bar/SFD phenomena are observed.

In this context, it should be taken into account that a significant correlations between SNe Ia decline rates (stretch parameters) and the global ages of hosts have been observed when the ages range from about 1 to ~ 10 Gyr (e.g. [Gupta et al. 2011](#); [Pan et al. 2014](#); [Campbell et al. 2016](#); [H20](#)). In the stacked discs of Sa–Scd galaxies, however, the azimuthally averaged age of the stellar population ranges roughly from 8.5 to 10 Gyr from the disc edge to the center, respectively (e.g. [González Delgado et al. 2015](#)). Most likely, this narrow average age distribution across the mean (stacked) host disc does not allow to see a significant correlation between the Δm_{15} and \tilde{r}_{SN} in Table 4.

It is clear that such a mean disc contains an overlaid components of old and young stars at any radius. On the other hand, as shown

in della Valle & Livio (1994); Aramyan et al. (2016), a considerable fraction of SNe Ia in spiral galaxies is (observationally) linked to the young/star-forming disc population, rather than to the population of old disc or bulge. These SNe Ia exhibit an average delay time of 200 – 500 Myr (prompt events, e.g. Raskin et al. 2009) and should have slower declining LCs (smaller Δm_{15} values, e.g. Shen et al. 2017). For this reason, the SNe Ia host disc is outnumbered by slower declining events outside the SFD (Fig. 2).

Given these results, we check the $\Delta m_{15} - \tilde{r}_{\text{SN}}/\tilde{r}_{\text{dem}}$ correlation for normal SNe Ia in the SFD+outer disc, bar/SF+outer disc, and combined samples. Table 4 shows that the mentioned correlation is statistically significant for the first sample, while it is not significant for the second and combined samples. Thus, the old SFD population ($\gtrsim 2$ Gyr), which contains mostly faster declining SNe Ia (larger Δm_{15}), in combination with the younger outer disc, which is outnumbered by SNe Ia with slower declining LCs (smaller Δm_{15}), cause the observed trend in the SFD+outer disc (Fig. 2 and Table 4).

4 CONCLUSIONS

In this *Letter*, using a sample of nearby Sa–Scd galaxies hosting 185 SNe Ia and our visual classification of the ionized (UV and/or H α) discs of the galaxies, we perform an analysis of the locations and LC decline rates (Δm_{15}) of normal and peculiar SNe Ia in the SFDs and beyond. As in earlier studies, we confirm that in the stacked spiral disc, the Δm_{15} of SNe Ia do not correlate with their galactocentric radii, and such disc is outnumbered by slower declining/prompt events. For the first time, we demonstrate that from the perspective of the dynamical timescale of the SFD, its old stellar population ($\gtrsim 2$ Gyr) hosts mostly faster declining SNe Ia ($\Delta m_{15} > 1.25$). By linking the LC decline rate and progenitor age, we show that the SFD phenomenon gives an excellent possibility to constrain the nature of SNe Ia. We encourage further analysis (e.g. integral field observations) using the SFD phenomenon on larger datasets of SNe Ia and their host galaxies to better constrain SN Ia progenitor ages.

ACKNOWLEDGEMENTS

We thank the anonymous referee for thoughtful comments and efforts towards improving our *Letter*. This work was made possible in part by a research grant from the Armenian National Science and Education Fund (ANSEF) based in New York, USA. V.A. is supported by FCT through national grants: UID/FIS/04434/2019; UIDB/04434/2020; UIDP/04434/2020, and Investigador contract nr. IF/00650/2015/CP1273/CT0001.

DATA AVAILABILITY

The data underlying this study are available in the *Letter*, in its online supplementary material (for guidance see Table A1), and in H20.

REFERENCES

Anderson J. P., James P. A., Förster F., González-Gaitán S., Habergham S. M., Hamuy M., Lyman J. D., 2015, *MNRAS*, **448**, 732
 Aramyan L. S., et al., 2016, *MNRAS*, **459**, 3130
 Barkhudaryan L. V., Hakobyan A. A., Karapetyan A. G., Mamon G. A., Kunth D., Adibekyan V., Turatto M., 2019, *MNRAS*, **490**, 718
 Blondin S., Dessart L., Hillier D. J., Khokhlov A. M., 2017, *MNRAS*, **470**, 157

Campbell H., Fraser M., Gilmore G., 2016, *MNRAS*, **457**, 3470
 Childress M. J., Wolf C., Zahid H. J., 2014, *MNRAS*, **445**, 1898
 Crocker R. M., et al., 2017, *Nature Astronomy*, **1**, 0135
 della Valle M., Livio M., 1994, *ApJ*, **423**, L31
 Di Matteo P., Haywood M., Combes F., Semelin B., Snaith O. N., 2013, *A&A*, **553**, A102
 Díaz-García S., Salo H., Laurikainen E., Herrera-Endoqui M., 2016, *A&A*, **587**, A160
 Díaz-García S., Moyano F. D., Comerón S., Knapen J. H., Salo H., Bouquin A. Y. K., 2020, *A&A*, **644**, A38
 Donohoe-Keyes C. E., Martig M., James P. A., Kraljic K., 2019, *MNRAS*, **489**, 4992
 Fisher R., Jumper K., 2015, *ApJ*, **805**, 150
 Galbany L., et al., 2012, *ApJ*, **755**, 125
 Gallagher J. S., Garnavich P. M., Berlind P., Challis P., Jha S., Kirshner R. P., 2005, *ApJ*, **634**, 210
 George K., Joseph P., Mondal C., Subramanian S., Subramaniam A., Paul K. T., 2020, *A&A*, **644**, A79
 González Delgado R. M., et al., 2015, *A&A*, **581**, A103
 Gupta R. R., et al., 2011, *ApJ*, **740**, 92
 Hakobyan A. A., et al., 2016, *MNRAS*, **456**, 2848
 Hakobyan A. A., Barkhudaryan L. V., Karapetyan A. G., Gevorgyan M. H., Mamon G. A., Kunth D., Adibekyan V., Turatto M., 2020, *MNRAS*, **499**, 1424 (H20)
 Han Z., Podsiadlowski P., 2004, *MNRAS*, **350**, 1301
 James P. A., Percival S. M., 2015, *MNRAS*, **450**, 3503
 James P. A., Percival S. M., 2018, *MNRAS*, **474**, 3101
 Kang Y., Lee Y.-W., Kim Y.-L., Chung C., Ree C. H., 2020, *ApJ*, **889**, 8
 Kasen D., Röpke F. K., Woosley S. E., 2009, *Nature*, **460**, 869
 Kennicutt Robert C. J., 1998, *ARA&A*, **36**, 189
 Livio M., Mazzali P., 2018, *Phys. Rep.*, **736**, 1
 Martin D. C., et al., 2005, *ApJ*, **619**, L1
 Minchev I., et al., 2018, *MNRAS*, **481**, 1645
 Pan Y. C., et al., 2014, *MNRAS*, **438**, 1391
 Panther F. H., Seitzzahl I. R., Ruiter A. J., Crocker R. M., Lidman C., Wang E. X., Tucker B. E., Groves B., 2019, *PASA*, **36**, e031
 Pavlyuk N. N., Tsvetkov D. Y., 2016, *Astron. Lett.*, **42**, 495
 Phillips M. M., 1993, *ApJ*, **413**, L105
 Raskin C., Scannapieco E., Rhoads J., Della Valle M., 2009, *ApJ*, **707**, 74
 Rigault M., et al., 2013, *A&A*, **560**, A66
 Roming P. W. A., et al., 2005, *Space Sci. Rev.*, **120**, 95
 Rose B. M., Garnavich P. M., Berg M. A., 2019, *ApJ*, **874**, 32
 Ruiter A. J., et al., 2013, *MNRAS*, **429**, 1425
 Sánchez-Menguiano L., et al., 2018, *A&A*, **609**, A119
 Shen J., Sellwood J. A., 2004, *ApJ*, **604**, 614
 Shen K. J., Toonen S., Graur O., 2017, *ApJ*, **851**, L50
 Shen K. J., Blondin S., Kasen D., Dessart L., Townsley D. M., Boos S., Hillier D. J., 2021, *ApJ*, **909**, L18
 Sim S. A., Röpke F. K., Hillebrandt W., Kromer M., Pakmor R., Fink M., Ruiter A. J., Seitzzahl I. R., 2010, *ApJ*, **714**, L52
 Timmes F. X., Brown E. F., Truran J. W., 2003, *ApJ*, **590**, L83
 Uddin S. A., Mould J., Lidman C., Ruhlmann-Kleider V., Zhang B. R., 2017, *ApJ*, **848**, 56
 Wang L., Höflich P., Wheeler J. C., 1997, *ApJ*, **483**, L29

SUPPORTING INFORMATION

Supplementary data are available at *MNRAS* online.

Table A1. The database of 185 individual SNe Ia and their 180 host galaxies.

Please note: Oxford University Press is not responsible for the content or functionality of any supporting materials supplied by the authors. Any queries (other than missing material) should be directed to the corresponding author for the article.

Table A1. The database (first 10 rows) of 185 SNe Ia and their 180 host galaxies. The full table is available as supplementary material.

| SN | Host | Morph. | Bar | Disc's class | Location | \tilde{r}_{SN} | \tilde{r}_{dem} |
|--------|---------------|--------|-----|--------------|------------|-------------------------|--------------------------|
| 1974G | NGC4414 | Sc | | <i>i</i> | disc | 0.425 | – |
| 1981B | NGC4536 | Sbc | | <i>i</i> | disc | 0.697 | – |
| 1982B | NGC2268 | Sc | B | <i>iii?</i> | outer disc | 0.267 | 0.150 |
| 1989A | NGC3687 | Sc | B | <i>iii:</i> | outer disc | 0.524 | 0.175 |
| 1989B | NGC3627 | Sb | B | <i>ii</i> | bar/SF | 0.171 | 0.200 |
| 1990N | NGC4639 | Sbc | B | <i>iii</i> | outer disc | 0.859 | 0.253 |
| 1990O | MCG+03-44-003 | Sbc | B | <i>iii?</i> | outer disc | 0.764 | 0.333 |
| 1991T | NGC4527 | Sbc | | <i>i</i> | disc | 0.518 | – |
| 1992bc | ESO300-009 | Scd: | | <i>i</i> | disc | 0.897 | – |
| 1992bg | PGC343503 | Sb: | | <i>i</i> | disc | 0.546 | – |

APPENDIX A: ONLINE MATERIAL

The database of our analysis is available in the online supplementary material of the *Letter*. The first 10 rows of the database of 185 SNe Ia (SN name, location, deprojected and R_{25} -normalized galactocentric distance) and their 180 hosts (galaxy name, morphological type, bar detection, disc's class, and demarcation radius) are shown in Table A1. The full table is available in an CSV format. Recall that more data on these SNe Ia and their host galaxies are available in H20 (e.g. SN spectroscopic subclass, Δm_{15} , galaxy distance).

This paper has been typeset from a $\text{\TeX}/\text{\LaTeX}$ file prepared by the author.